Design considerations for the drive system of an ultra-high speed spinning ball motor

C. Wildmann*, T. Nussbaumer**, J. W. Kolar*

* ETH Zurich, Power Electronics Systems Laboratory, 8092 Zürich, Switzerland
** Levitronix GmbH, 8005 Zürich, Switzerland

Abstract-- **This paper presents considerations for the drive system of a magnetically levitated ultra-high speed spinning ball motor. The system shall provide rotation speeds in the range of several million rotations per minute in future. In a first approach, the functionality is analyzed and verified on a system, which is enlarged by a factor of four compared to the motor size which shall provide the targeted rotational speed of the rotor. Possibilities of improvement for the final drive design are investigated in detail by using 3D FEM analysis. Finally, a new coreless drive unit, which shall provide higher rotor speeds of smaller rotors, is developed.**

Index Terms-- **Asynchronous drive, magnetic bearing, spinning ball, ultra-high speed**

I. INTRODUCTION

All electrical equipment shows a clear tendency towards smaller sizes, compactness and high efficiency. In order to provide the power necessary to fulfill a purpose of the motor the rotational speed of small rotors has to be increased significantly. In the range of several million rpm (rotations per minute) additional problems regarding rotor sizes measured in tenth of millimeters, vibrations and large friction are introduced, hereby opening up a new territory of interesting and necessary research.

The ultimate limit of rotational speed is given by the load limit of the rotor material. Forces acting on the rotor at certain rotational speeds can be reduced by reducing the rotor diameter. At some point the detection and control of sub-millimeter sized rotors becomes hardly feasible. To defer this limit and overcome challenges related to rotor shape and motor design, choice of rotor material and rotor damping represent a major challenge along with the main goal of breaking the rotational speed record of 23.16 mio rpm which was achieved by J.W. Beams [1] in 1946 with a rotor diameter of $d = 0.8$ mm. The rotor supposedly withstood stresses up to 2.9 GPa. This value appears to be very high for the state of technology at this point and has surprisingly never been reached again. Therefore, this value has often been questioned, although a possible explanation of this result can be found in [2].

So far, no one else ever made it anywhere near the mentioned speed. The last attempt to comprehend and outperform the record has been published in 2005 by A.R. Boletis [3]. His experimental conditions allowed the rotor to reach a maximum speed of 2.88 mio rpm, which was limited by the poor vacuum, as stated by the author.

The maximum attainable speed was estimated to be at around 10 mio rpm with a vacuum in the range of less than a tenth of a μbar.

Already as early as in 1941 L.E. MacHattie [4] and J.W. Beams were already experimenting with very small, magnetically bedded rotors in vacuum, which they accelerated up to the range of millions of revolutions per minute (rpm). Table I gives a short overview over the highest rotational speeds ever reached.

TABLE I
OVERVIEW OVER THE WORK ALREADY DONE AND THEIR RESULTS.

Year	1941	1946	2005
Name	L.E. MacHattie	J.W. Beams	A.R. Boletis
Rot. speed	6.6 mio rpm	23.16 mio rpm	2.88 mio rpm
Diameter	2.38 mm	0.8 mm	1 mm
Rotor stress	2.2 GPa	2.9 GPa	75.6 MPa
Pressure	0.067 μbar	0.013 μbar	0.05 mbar
Speed limited by	Electronics	Load limit of the rotor	Friction, possibly electronics

II. PRELIMINARY TEST SETUP

In order achieve the main goal of this project, which is to break the world record in rotational speed (23.16 mio rpm), a two-step procedure was followed to find an optimal drive design for the ultra-high speed motor.

In a first step an experimental setup shown in Fig.1 was developed to investigate the magnetic bearing properties along with the sensor system, the effect of high-order harmonics originating from the drive coils on the rotor stability and the effect of passive and active damping on radial rotor vibrations. In the following, the main focus will be put on the analysis and appropriate design of the drive system.
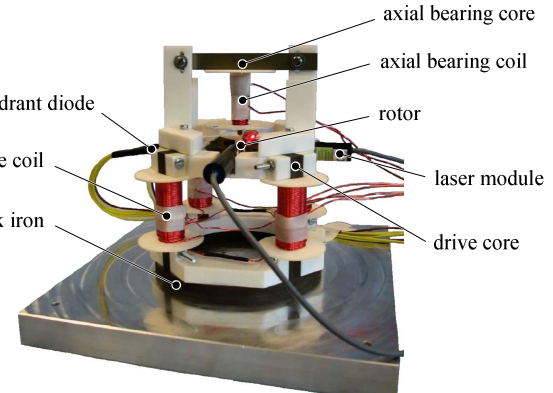
Fig. 1. First preliminary test setup of the ultra-high speed motor.
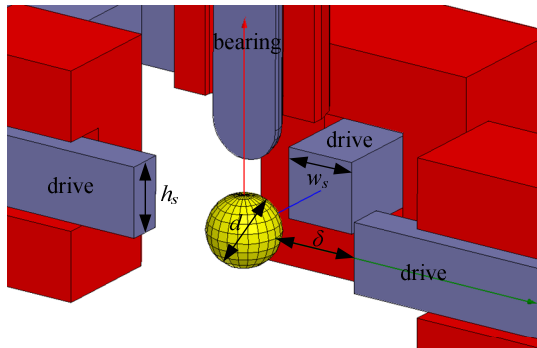
Fig. 2. Parameters describing the configuration of the first prototype.

Fig. 3. Schematic setup to control all degrees of freedom and still defining a preferred position of the rotor in the motor center by using a damping needle below the rotor.

Fig. 4. Rotor ($d = 4$ mm, with passive damping by damping needle) stably spinning at 60'000 rpm.

In order to analyze the effect of single harmonics, one design criterion of the drive units was the creation of a purely sinusoidal B-field around the rotor if the drive teeth are fed by sinusoidal currents. Fig. 2 shows the parameters of the drive units influencing the magnetic field shape around the rotor, namely the height h_s and the width w_s of the stator and the air gap δ. Another design criterion was that small radial displacements of the rotor towards the drive cores shall keep the relative change of the air gap δ small. This way it is ensured that the destabilizing force acting on the rotor stays as small as possible as well.

These preconditions led to a comparatively large design (drive core dimensions are: $h_s = 8$ mm, $w_s = 9$ mm and $\delta = 10$ mm), which also required a large rotor ($d = 4$ mm). This represents a factor of four compared to the rotor which shall provide the final rotational speed. Obviously, this setup is not suitable to reach very high rotational speeds, but it is convenient for a first test setup also because potential problems of miniaturization, such as rotor detection, rotor handling and the ability of optical observation of the rotor can be avoided.

Experiments have shown that the rotor can be passively stabilized very well in the xy-plane by using a damping needle placed underneath the rotor (cf. Fig. 3). Furthermore, high-order harmonics above 100 Hz do not excite any rotor instability. This relates to the fact that for a future design the creation of a sinusoidal magnetic field is not a requirement. For this setup, a rotor speed of 60'000 rpm (see Fig. 4) has been reached. The rotor speed was determined by measuring reflections of the rotor which was possible due coloring one half of the surface with a conventional marker.

Furthermore, the investigation showed that iron losses become considerable already at comparable low frequencies. At a rotary field of 1.5 kHz and a magnetic field density in the drive cores of 1 T the temperature reaches 50°C (switching frequency: 35 kHz). This is the reason why in the final design (cf. section IV) new drive units without an iron core are designed to reach the objective of breaking the rotational speed record. The development of these units is then carried out already for the targeted rotor diameter of $d = 1$ mm.
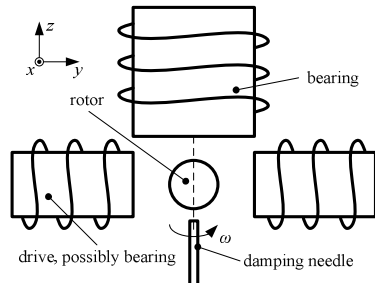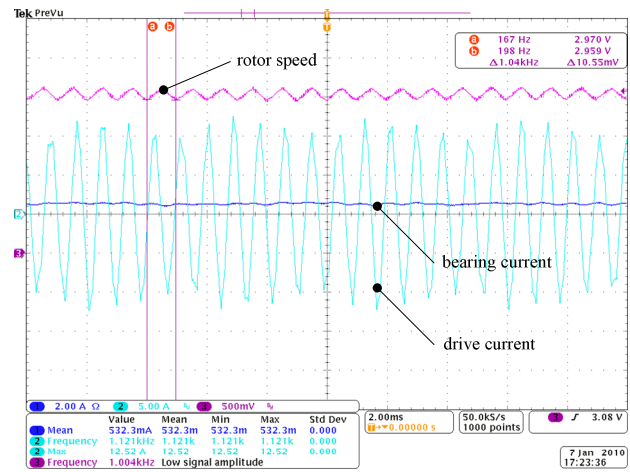
III. DRIVE CONCEPT

By using contactless magnetic bearings and having the rotor in a vacuum the main obstacle standing in the way of high speeds - the friction - is eliminated. In order to be able to levitate and spin the rotor it has to be ferromagnetic. This fact rules out strong rotor materials as carbon nanotubes and leaving high strength steel and metallic glasses as the only materials to go with. Since the rotor is very small (range of a few millimeters), it has to be made out of one piece of material. This condition leads to an electrical machine concept known as asynchronous brushless motor.

In the following, the physical and mathematical background for this kind of rotor is explained in order to understand the drive mechanisms and limitations and draw the appropriate conclusions for the final drive design.

To describe the electromagnetic force and torque acting on the rotor all variables are transformed into quantities in a coordinate system rotating with the rotation speed and are indicated with an "r" in subscript. The following considerations are based on a simplified model having a spherical solid steel rotor with diameter d in an external magnetic rotary field described with a constant frequency ω_s and with a constant magnetic field density $\mathbf{B}_r$ defined

by the two phase drive units of the stator in the rotor coordinate system. A schematic visualization is given in Fig. 5. The boundary conditions in formulas are the following:

$$\boldsymbol{\omega}_s = \omega_s \begin{pmatrix} 0 \\ 0 \\ 1 \end{pmatrix} \qquad (1)$$

$$\boldsymbol{\Phi}_r = \eta \cdot \boldsymbol{\Phi}_s = \eta \cdot A_s \cdot \mathbf{B}_s = \eta \cdot w_s \cdot h_s \cdot \mathbf{B}_s \qquad (2)$$

$\boldsymbol{\Phi}_r$: rotor flux
$\boldsymbol{\Phi}_s$: stator flux generated by current in the drive coils
η: coupling factor describing the relation between rotor flux and stator flux in percent [%]
A_s: cross-sectional area of the drive iron core

It is assumed that the stator current $\mathbf{I}_s$ has a constant amplitude as well, which is achieved by adjusting the stator voltage $\mathbf{U}_s$, which is given by

$$\mathbf{U}_s = \mathbf{U}_{s,0} - \mathbf{U}_{ind,s} = \mathbf{U}_{s,0} + N \frac{\eta \cdot \boldsymbol{\Phi}_r}{\mathrm{d}t} . \qquad (3)$$

$\mathbf{U}_s$: actual stator voltage.
$\mathbf{U}_{s,0}$: stator voltage necessary to create a rotor flux $\mathbf{B}_r$ while no power is transferred on the rotor.
$\mathbf{U}_{ind,s}$: electromotive force generated in the stator drive coils caused by the eddy currents on the rotor.
N: number of turns of one drive phase.

Introducing a rotating coordinate system as shown in Fig. 5, where the x-axis is parallel to the B-field generated, the rotor flux $\boldsymbol{\Phi}_r$ can be written as

$$\boldsymbol{\Phi}_r = A_r \cdot \mathbf{B}_r = A_r \cdot B_r \begin{pmatrix} 1 \\ 0 \\ 0 \end{pmatrix}, \qquad (4)$$
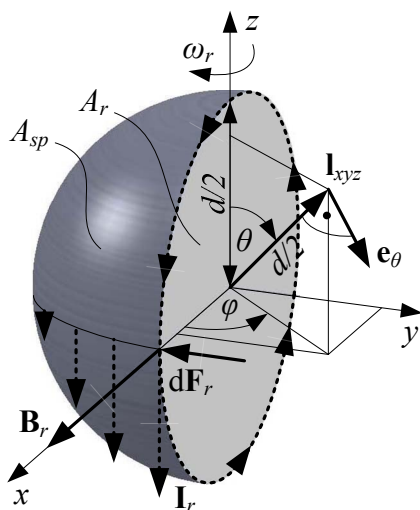
Fig. 5. Description of the variables used to calculate the rotor torque.

where A_r is the cross section of the rotor and $\mathbf{B}_r$ the magnetic flux density in the rotor.

According to Faraday's law of induction the electromotive force $\mathbf{U}_{ind,r}$ induced in the rotor as a one turn wire is given by

$$\mathbf{U}_{ind,r} = -\frac{\mathrm{d}\boldsymbol{\Phi}_r}{\mathrm{d}t} = -A_r \frac{\mathrm{d}\mathbf{B}_r}{\mathrm{d}t} = -\pi \left(\frac{d}{2}\right)^2 \frac{\mathrm{d}\mathbf{B}_r}{\mathrm{d}t} . \qquad (5)$$

Formula (5) written in the frequency domain is

$$\mathbf{U}_{ind,r} = -\mathrm{j}\omega \cdot \boldsymbol{\Phi}_r = -\mathrm{j}\omega \cdot \mathbf{B}_r \cdot A_r = -\mathrm{j}\omega \cdot \mathbf{B}_r \cdot \pi \left(\frac{d}{2}\right)^2 , \qquad (6)$$

where ω is the difference between the rotational speed of the rotary field ω_s and the actual rotational speed of the rotor ω_r:

$$\boldsymbol{\omega}_r = \omega_r \begin{pmatrix} 0 \\ 0 \\ 1 \end{pmatrix}, \qquad (7)$$

$$\omega = \omega_s - \omega_r . \qquad (8)$$

The slip s is by definition

$$s = \frac{\omega_s - \omega_r}{\omega_s} = \frac{\omega}{\omega_s} , \qquad (9)$$

wherefore ω can be substituted with

$$\omega = s \cdot \omega_s . \qquad (10)$$

The rotor current $\mathbf{I}_r$ generated by the electromotive force $\mathbf{U}_{ind,r}$ is determined by the resistance R_r and the inductance L_r of the rotor and is calculated as

$$\mathbf{I}_r = \frac{\mathbf{U}_{ind,r}}{R_r + \mathrm{j}\omega \cdot L_r} . \qquad (11)$$

$\mathbf{I}_r$ will occur on the surface of the solid steel ball as indicated by the dashed loop in Fig. 5, since all eddy currents inside the rotor cancel each other out. Furthermore, $\mathbf{I}_r$ has a phase shift close to 90° degrees compared to the external rotary field assuming a small rotor inductance L_r.

The distribution of the skin-deep rotor current is sinusoidal. Its amplitude can be described with a location dependent term $I_r \cdot \cos(\varphi)$ and its direction is always tangential to the surface described with the unit vector $\mathbf{e}_\theta$. The variables φ and θ represent spherical coordinates, as illustrated in Fig. 5. With this, the current is

$$\mathbf{I}_r = I_r \cdot \cos(\varphi) \cdot \mathbf{e}_\theta , \qquad (12)$$

where

$$\mathbf{e}_\theta = \begin{pmatrix} \cos(\theta)\cos(\varphi) \\ \cos(\theta)\sin(\varphi) \\ -\sin(\theta) \end{pmatrix}. \qquad (13)$$

Forces acting on an infinitesimal small surface of the rotor $d\mathbf{F}_r$ are calculated using the formula for the Lorentz force:

$$d\mathbf{F}_r = I_r \cdot \cos(\varphi) \cdot \frac{d}{2}(\mathbf{e}_\theta \times \mathbf{B}_r) \cdot d\theta \cdot \frac{d}{2} \cdot \sin(\theta) \cdot d\varphi. \quad (14)$$

Using

$$dA_{sp} = \left(\frac{d}{2}\right)^2 \cdot \sin(\theta) \cdot d\theta \cdot d\varphi \qquad (15)$$

formula (14) can be written with (4), (13) and (15) as

$$d\mathbf{F}_r = I_r \cdot \cos(\varphi) \cdot \left(\begin{pmatrix} \cos(\theta)\cos(\varphi) \\ \cos(\theta)\sin(\varphi) \\ -\sin(\theta) \end{pmatrix} \times \begin{pmatrix} B_r \\ 0 \\ 0 \end{pmatrix} \right) \cdot dA_{sp} \quad (16)$$

The cross product solved:

$$d\mathbf{F}_r = I_r \cdot B_r \cos(\varphi) \cdot \begin{pmatrix} 0 \\ -\sin(\theta) \\ -\cos(\theta)\sin(\varphi) \end{pmatrix} \cdot dA_{sp} \qquad (17)$$

The rotor torque $d\mathbf{M}_r$ generated defined by the cross product of the displacement vector $\mathbf{l}_{xyz}$ and the force $d\mathbf{F}_r$:

$$d\mathbf{M}_r = \mathbf{l}_{xyz} \times d\mathbf{F}_r = \frac{d}{2}\begin{pmatrix} \sin(\theta)\cos(\varphi) \\ \sin(\theta)\sin(\varphi) \\ \cos(\theta) \end{pmatrix} \times d\mathbf{F}_r. \qquad (18)$$

Solving the cross product we find

$$d\mathbf{M}_r = C_1 \cos(\varphi)\begin{pmatrix} \cos(\theta)\sin(\theta)\left(1-\sin^2(\varphi)\right) \\ \sin(\varphi)\cos(\varphi)\cos(\theta)\sin(\theta) \\ \sin^2(\theta)\cos(\varphi) \end{pmatrix} \cdot dA_{sp}, (19)$$

where

$$C_1 = I_r \cdot B_r \frac{d}{2}. \qquad (20)$$

The integral of calculating the surface A_{sp} of the spherical rotor is given by

$$A_{sp} = 2\int_{-\frac{\pi}{2}}^{\frac{\pi}{2}}\int_0^\pi \left(\frac{d}{2}\right)^2 \cdot \sin(\theta) \cdot d\theta \cdot d\varphi. \qquad (21)$$

Therefore, the rotor torque $\mathbf{M}_r$ is

$$\mathbf{M}_r = C_2 \int_{-\frac{\pi}{2}}^{\frac{\pi}{2}}\int_0^\pi \begin{pmatrix} \cos^3(\varphi)\cos(\theta)\sin^2(\theta) \\ \sin(\varphi)\cos^2(\varphi)\cos(\theta)\sin^2(\theta) \\ \cos^2(\varphi)\sin^3(\theta) \end{pmatrix} d\theta \cdot d\varphi, \quad (22)$$

where

$$C_2 = C_1 \frac{d^2}{2}. \qquad (23)$$

The solved integral leads to

$$\mathbf{M}_r = C_2 \begin{pmatrix} 0 \\ 0 \\ \frac{2\pi}{3} \end{pmatrix} = I_r \cdot B_r \cdot d^3 \frac{\pi}{6}\begin{pmatrix} 0 \\ 0 \\ 1 \end{pmatrix}. \qquad (24)$$

The power transferred on the rotor is given by

$$P = \mathbf{M}_r^T \cdot \boldsymbol{\omega}_r = \mathbf{U}_{ind,s}^T \cdot \mathbf{I}_s. \qquad (25)$$

By combining (25) with (24), (6), (11) and assuming low rotor inductance L_r, the following relation applies:

$$P \propto \mathbf{M}_r \propto \frac{\omega \cdot B_r^2 d^5}{R_r} \qquad (26)$$

Relation (26) can be used as a guideline for designing the new drive units. To have a maximal power transferred on the rotor $\mathbf{M}_r$ has to be maximized. This is the case, if the magnetic flux density B_r is maximal. B_r can be directly influenced by the geometry of the drive units. The efficiency of the motor can be increased by a low resistance material rotor coating. This way the losses on the rotor are minimized. As an alternative to geometry related improvements also the stator frequency ω_s can be increased.

The preliminary test setup creates a magnetic flux density of $B_r = 70$ mT at a current density of the drive coils of $J_d = 3$ A/mm^2 and a drive coil cross-sectional area of 160 mm^2. To make the rotor spin, B_r has to reach a value of at least 3.5 mT.

IV. Development of Final Ultra-High Speed Design

Because of the lack of iron cores the magnetic field cannot be arbitrarily conducted anymore. Therefore, it is important to place the drive coils as close as possible to the rotor ($d = 1$ mm), which leads to the cone-shaped drive coils illustrated in Fig. 6. The air gap δ is fixed to $\delta = 3$ mm, smaller values would lead to problems regarding the integration of a pressure-resistant vacuum hose later. Parameters used for the optimization are
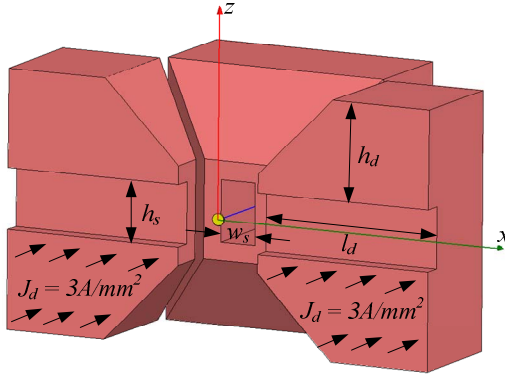
Fig. 6. Cross-section of the setup showing the parameters used for the drive unit optimization for the final setup ($d = 1$ mm).

Fig. 7. Magnetic field density B_r in the rotor depending on the inner coil dimensions w_s and h_s ($l_d = 15$ mm, $h_d = 9$ mm, $J_d = 3$ A/mm^2).

TABLE II
VARIABLES AND THEIR NOMINAL VALUES USED FOR THE DRIVE UNIT OPTIMIZATION.

Parameter	Description	Nominal value
h_s	inner height of the drive coil	4 mm
w_s	inner width of the drive coil	2 mm
h_d	height of the drive coil	9 mm
l_d	length of the drive coil	15 mm

illustrated in Fig. 6; their nominal values are given in Table II.

All following 3D FEM simulation results are given for a current density of $J_d = 3$ A/mm^2 with uniform distribution over the cross-sectional area of each active drive coil as shown in Fig 6.

To understand the following results it is important to keep in mind that in this setup the cross-sectional area of the drive coils is dependent on some of the parameters used for optimization. For instance a larger inner coil width w_s leads to less space available for the actual coil and therefore the generated magnetic field B_r becomes smaller due to the lower value of impressed ampere-turns. Fig. 7 shows the dependence on inner coil dimensions. To maximize B_r the inside of the coil has to be small in its width and large in its height. Since the rotor is held in the air by an electromagnet placed above the drive units, h_s has to be limited. Otherwise the bearing system lies too far away from the rotor to affect its z-position. As the tendency in Fig. 7 shows, at some point the enlargement of h_s becomes irrelevant anyway.

The effect of the drive coil length l_d on the magnetic flux density B_r in the rotor shows a flattening effect towards larger drive coil lengths. Anyway, also here it makes sense to limit its value in order to keep the inductance of the stator small. Simulation results are presented in Fig. 8.

As Fig. 9 shows, the height of the drive coil h_d has the largest influence on the magnetic flux density B_r in the rotor. Although again a flattening effect towards larger coil height values is observable, it is less distinct than the characteristics before. Nevertheless, this value has to be
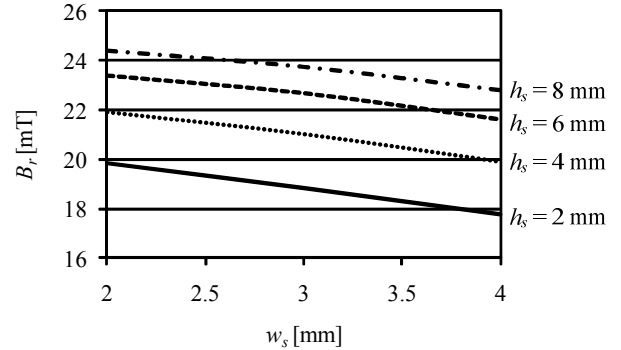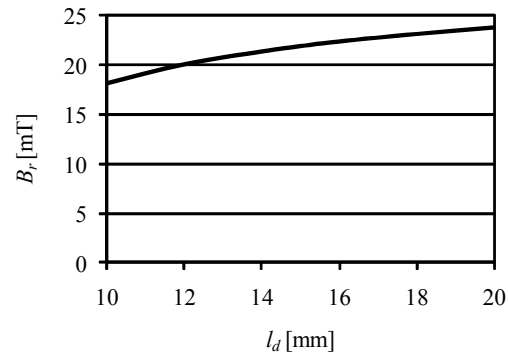
Fig. 8. Magnetic field density B_r in the rotor depending on the drive coil length l_d ($w_s = 2$ mm and $h_s = 4$ mm, $h_d = 9$ mm, $J_d = 3$ A/mm^2).
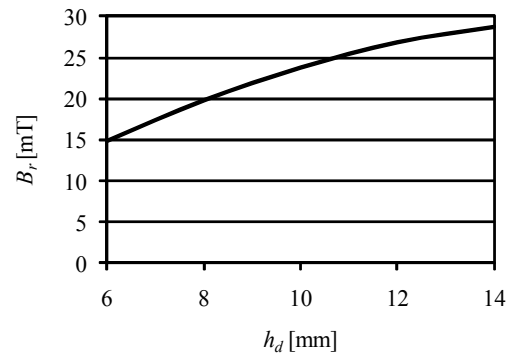
Fig. 9. Magnetic field density B_r in the rotor depending on the drive coil height h_d ($w_s = 2$ mm and $h_s = 4$ mm, $l_d = 15$ mm, $J_d = 3$ A/mm^2).

limited as well because of the bearing coil above the drive setup, which must not lie too far from the rotor in order to fulfill its purpose.

The resulting drive setup is shown in Fig. 10 with all its dimensions. The coreless drive units generate a B-field of $B_r = 35$ mT in the rotor. With this, a very efficient coreless drive setup has been found being suitable for the realization of multi-million rpm spinning ball motor. The integration of ferrite cores into the configuration is not recommendable due to the large iron losses but remains a possibility and will be investigated in the future.
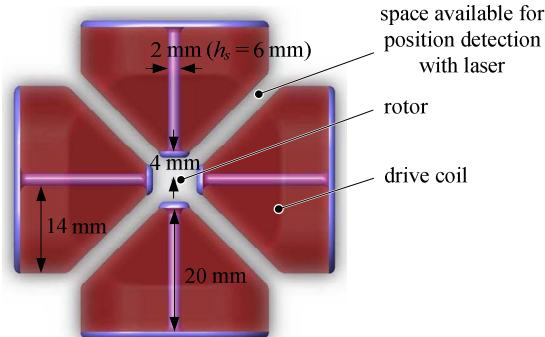
Fig. 10. Coreless drive geometry of the second prototype.

V. CONCLUSIONS

This paper has presented design considerations for an an ultra-high speed spinning ball motor. A preliminary test setup with increased dimensions allowed valuable insights into design-related guidelines of the future motor and showed that the rotor can be stabilized passively in the *xy*-plane using a damping needle. Subsequently, the drive concept has been explained in detail and the influence of different parameters on the rotor power transfer has been revealed. Since iron losses become considerable at the target frequency (several 100 kHz) of the rotary field, new coreless drive units are designed.

The next step includes the fabrication of the second prototype and its experimental evaluation.

REFERENCES

[1] Beams, J.W.; Young, J.L. III; Moore, J.W.: *The Production of High Centrifugal Fields*. In: Journal of Applied Physics 17 (1946), Nr. 5, S. 886–890

[2] Beams, J.W.; Breazeale, J.B.; Bart, W.L.: *Mechanical Strength of Thin Films of Metals*. In: *Physical Review* 100 (1955), Nr. 6, S. 1657–1661.

[3] Boletis, A.R.:High Speed Micromotor on a Three Axis Active Magnetic Bearing, École Polytechnique Fédérale de Lausanne, Diss., 2005. – Nr. 3160

[4] MacHattie, L.E.: *The Production of High Rotational Speed*. In: Review of Scientific Instruments 12 (1941), S. 429

[5] Wang, W.H.; Dong, C.; Shek, C.H.: *Bulk metallic glasses*. In: Materials Science & Engineering R 44 (2004), Nr. 2-3, S. 45–89

[6] Inoue, A.: *Stabilization of metallic supercooled liquid and bulk amorphous alloys*. In: Acta materialia 48 (2000), Nr. 1, S. 279–306

[7] Inoue, A.; Shen, B.L.; Koshiba, H.; Kato, H.; Yavari, AR: *Ultra-high strength above 5000 MPa and soft magnetic properties of Co–Fe–Ta–B bulk glassy alloys*. In: Acta Materialia 52 (2004), Nr. 6, S. 1631–1637